Investigating the heat input effect of the GTAW process upon the microstructure and HAZ extension of HSLA-100 steel weld joints using thermal cycles

M. Darivandpour [1], R. Dehmolaei *[2], K. Ranjbar [3]

Department of Material science & Engineering, Faculty of Engineering, Shahid Chamran University of Ahvaz, Ahvaz, Iran

Abstract

In the present research, the welding of HSLA-100 steel was accomplished with three different heat inputs using the GTAW procedure. The microstructure of the disparate joint zones was examined utilizing an optical microscope and scanning electron microscope. To assess the impact of thermal cycles upon the extension and changes in the heat-affected zone, the thermocouples were placed at distinct distances from the fusion line. The results revealed that the weld metal microstructure consists of acicular ferrite and some polygonal and quasi-polygonal ferrites with the M/A constituent. An epitaxial growth was observed in the fusion line in all the heat inputs. It was determined that the heat-affected zone microstructure comprises two regions, namely a coarse-grained heat-affected zone with a granular and lath bainite microstructure and a fine-grained heat-affected zone with the prevailing microstructure of granular Bainite. The results indicated that the increasing of the heat input leads to a decrease in the amount of acicular ferrite and M/A constituent volume fraction in the weld metal and an increase in lath bainite in the coarse-grained zone. It was found that by increasing the heat input from 0.78kJ/mm to 1.42 kJ/mm, the grain size increases from 29.2 µm to 76.5 µm and from 15.7µm to 32.5µm in the coarse-grained and fine-grained zones, respectively. The thermal cycles evaluation pertinent to the implanting of a thermocouple disclosed that the heat-affected zone width is extended from 3.6 mm to 4.5mm by increasing the heat input from 0.78 kJ/mm to 1.42 kJ/mm.

Keywords:HSLA-100 steel, Microstructure, Thermal cycles, Granular bainite, Acicular ferrite, M/A constituent.

1. Introduction

High-strength low alloy steels (HSLA) are extensively used in the fabrication of diverse structures such as bridges, shipbuilding, gas, and oil transmission pipelines, submarine construction, and military industries owing to the appropriate combination of high strength and toughness. Due to the large scale of these structures, it is inevitable that they are connected using the welding process[1-3]. At first, the alloys used in shipbuilding and other types of military equipment were chosen from the low or medium carbon quenching and tempered steels. A group of these steels, such as HY-80 and HY-100, known as high yield (HY) steels, possesses high carbon content and high carbon equivalent values. These conditions, despite providing high strength for mentioned alloys, lead their coarse-grained heat-affected zone to be susceptible to hydrogen-induced cracking (HIC). For this reason, these alloys are not easily weldable and suffer from the low weldability. Accordingly, a new generation of copper-containing high-strength low alloy

**Corresponding author*
Email:Dehmolaei@scu.ac.ir
Address: Department of Material science & Engineering, Faculty of Engineering, Shahid Chamran University of Ahvaz, Ahvaz, Iran
1. Ph.D. Student
2. Assistant professor
3. Professor

steels, such as HSLA-100,has been developed, which possesses better weldability than HY steels. This steel has a lower carbon content (less than 0.1%) compared to the former grades (HY steels), and its strength loss due to a reduced carbon content is compensated for by the formation of the copper-rich precipitates, as well as Niobium, Titanium and Vanadium Carbonitrides. The carbon reduction in the HSLA steels compared to HY steels has improved toughness, weldability, and reduced production costs since it does not require preheating before welding. The proper chemical composition and desirable properties of this steel have caused it to be used as an alternative to HY-100 steel to construct warships and military equipment [4-8].

The microstructure of the weld metal and the heat-affected zone (HAZ) plays an important role in the quality and weld properties such as strength, toughness, and corrosion resistance [9]. The final microstructure formation of the welded joints is affected by various factors such as the welding thermal cycles (the heat input and cooling rate), base and filler metals chemical composition, the grain size of base metal, number of welding passes, and cooling rate after Ar3 temperature. A proper welding process and the accurate selection of welding parameters play an effective role in achieving the desired weld joint quality for a specific alloy. One of the important welding parameters is the heat input, which is a determinant factor in controlling and forming the weld metal and HAZ microstructure. The heat input affects the welding thermal cycles, cooling rate, and phase transformations in the weld metal and HAZ, as well as the formation and dissolution of precipitates (Carbides, Nitrides, and secondary phases [10].

Researches have shown that several microstructures can be formed in the HSLA-100 steel different joint zones (weld metal and HAZ) under different welding conditions. These microstructures tend to include kinds of ferrite (grain boundary, widmanstatten, polygonal and acicular), bainite, pearlite, martensite, and martensite/austenite (M/A) secondary phase or their combinations [11-13]. Using the GMAW procedure and ARC100 ultra-low carbon filler metal in the HSLA-100 steel welding, Spanos et al. [14],concluded that the weld metal microstructure is composed of acicular ferrite, which shows lower hardness compared to the base metal with lath martensite microstructure. Prasad zand Dwivedi [15] showed that by increasing the heat input of the submerged arc welding (SAW) process, the weld metal grain size is increased, resulting in the hardness reduction. Their results also revealed that the weld metal stiffness is altered by a change in the grain size. In a study conducted by Beidokhti et al. [16], it was found that the resistance to stress corrosion cracking and hydrogen-induced cracking is increased by increasing the acicular ferrite fraction in the HSLA-100 steel weld metal microstructure. Shome [17] illustrated that the austenite grain size in HAZ is increased and that the martensite packets and the acicular ferrite are also enlarged in this zone by increasing the heat input in HSLA-100 steel weld joints. Shome and Mohanti [18] investigated the effect of the two simulated 10 kJ/cm and 40 kJ/cm heat inputs on the microstructure of the heat-affected zone of HSLA-100 steel. It was determined that the austenite grain size during different thermal cycles affects the ferrite formation rate during the transformation. For this reason, the smaller the grain size in the microstructure is, the faster the transformation occurs. It was also elucidated that the HAZ microstructure comprises acicular ferrite and lath martensite, and that the acicular ferrite content is increased owing to lowering the cooling rate, which was the result of increasing heat input. Dong et al. [19] stated that the HSLA-100 steel HAZ microstructure mainly consists of martensite and that the microstructure is changed to bainite and some acicular ferrite by increasing the heat input. In this research, the influence of the GTAW process heat input on the microstructural changes, hardness, and HAZ expansion of the HSLA-100 steel welds has been studied using the welding thermal cycles and optical and scanning electron microscopes.

2. Materials and Experimental Procedure

In this study, the HSLA-100 steel plate with 9 mm thickness was produced under the controlled thermo-mechanical rolling conditions followed by quenched and tempered heat treatment at 950°C and 750°C, respectively. The applied welding consumable was the ER120S-G filler wire with a diameter of 2.4 mm. The weld coupons with dimensions of 100 mm × 50 mm were machined and separated from the HSLA-100 steel plate. A single V groove with an angle of 70°, a root face of 1 mm, and a root opening of 2 mm was employed as the butt weld joint configuration. The chemical composition of the base metal and the filler metal has been presented in Table 1.

Table 1. Chemical composition of base and filler metals (wt. %).

Materials	C	Mn	P	S	Si	Cr	Mo	Ni	Cu	Nb
HSLA-100	0.05	0.78	0.007	0.003	0.28	0.62	0.58	3.47	1.54	0.04
ER120S-G	0.08	1.45	0.002	0.003	0.6	-	0.55	3.4	-	-

The welding process was performed perpendicularly to the rolling direction by GTAW technique with a direct current electrode negative (DCEN) polarity in the four passes without applying any preheating in three different 0.78 Kj/mm, 1.22 Kj/mm, and 1.42 Kj/mm heat inputs. The argon gas with a 99.5% purity was used with flow rates of 15 L/min and 10 L/min for the purpose of shielding the cap and the root passes, respectively. The heat input of the welding was calculated by the formula (1) [20]:

$$H.I=\eta\frac{V.I}{1000S} \quad \text{Eq. (1)}$$

Where the V, I, S, and η are the welding voltage, the welding current, the welding speed, and the arc efficiency, respectively. Here, the arc efficiency is taken 70% for the GTAW procedure. The welding parameters have been summarized in Table 2. The thermocouple implantation was used to investigate the heat distribution in the area adjacent to the weld pool and its effect on the width of the heat-affected zone. For this purpose, eight Type K thermocouples with a diameter of 1.5 mm were utilized. For the implantation of the thermocouples, eight holes with a diameter of 1.5 mm and a depth of 3 mm were made on the root side of the joint. The first hole was created at a distance of 3.75 mm from the joint edge in the weld root zone, and the subsequent holes were made perpendicularly to the weld groove at a distance of 2 mm from the center of the adjacent holes in one direction. Inserting the thermocouple strings into the holes and connecting them to a data logger device made by Novus Company allowed for the recording of temperature changes versus time at different distances from the fusion line. The schematic image of the joint design and thermocouple locations has been shown in Fig. 1.

For microstructural examinations, samples with the size of 30 mm× 10 mm were cut from weldments so that the weld zone was located in the middle of each sample. The specimens were prepared by grinding using 60 to 2000 grits of SiC paper and then were followed by polishing by use of 1 μm Alumina powders. After polishing, the specimens were etched by a 2% nital solution reagent to reveal the microstructure of different zones. The lepera solution (with equal proportions of 1% sodium metabisulfite and 4% picral solutions) was used to detect M/A constituents [21]. The microstructure was studied by optical (OM) and scanning electron microscopes (SEM). The M/A constituent volume fraction in the weld metal was calculated using Image J and MIP soft wares. The primary austenite grain size in the heat-affected zone was determined by the intercept method according to ASTM E112-04 [22]. Vickers micro-hardness test was performed under a 100 g load to obtain the hardness profile at different distances from the fusion line.

3. Results and discussion

3.1. Microstructural study

The base metal microstructure and different weld

Table 2. Welding parameters.

Welded sample	Voltage(V)	Current(A)	Average Welding speed(mm/s)	Average heat-input(Kj/mm)
1	15	130	1.54	0.78
2	15	145	1.15	1.22
3	15	160	1.06	1.42

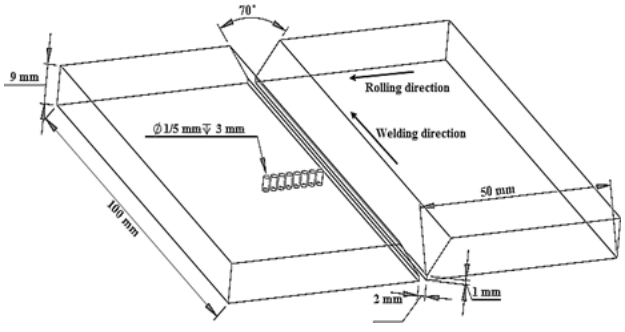

Fig. 1. Schematic of the joint design and thermocouples location.

zones have been investigated in this section.

3.1.1. Base metal microstructure

Fig. 2 shows the OM and SEM images of the HSLA-100 steel base metal microstructure. It can be observed that the base metal predominant microstructure consists of tempered lath martensite (LM) and granular Bainite (GB). The etching of the base metal by the Lepera solution shows M/A constituents formation in the matrix (Fig. 2-b). The incomplete transformation of austenite to martensite and bainite causes austenite to exist in some areas of the matrix as retained austenite. Some portion of retained austenite during the final stage of solidification is transformed into martensite and forms the M/A constituent [23]. More details of the microstructure and the presence of M/A constituent can be observed in the SEM image in Fig. 2-c. Similar results have been obtained by other researchers [4,5].

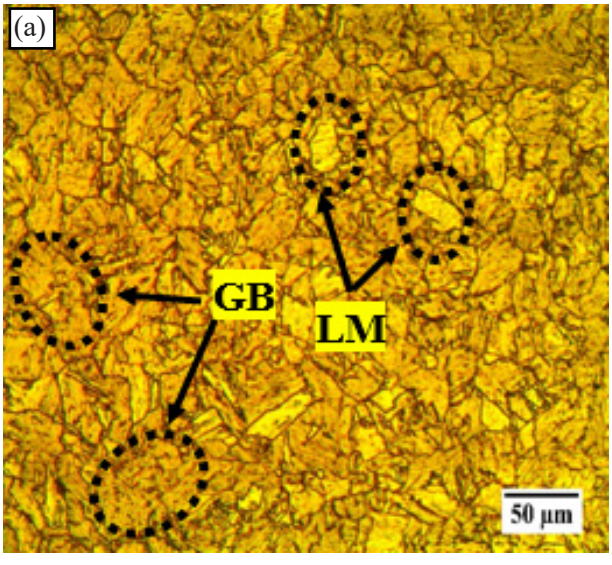

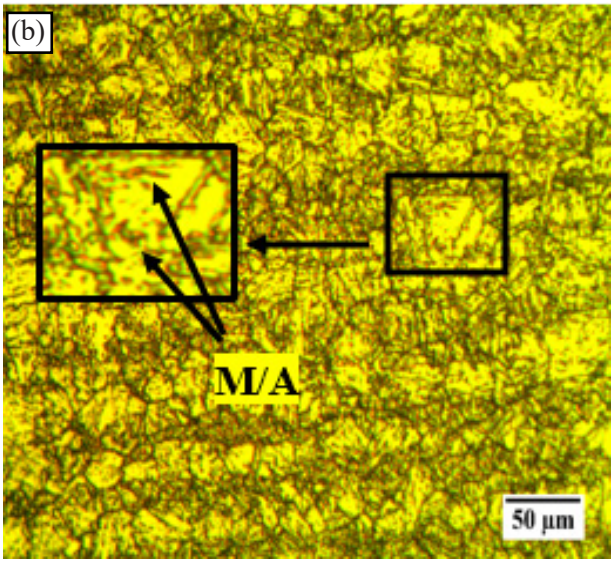

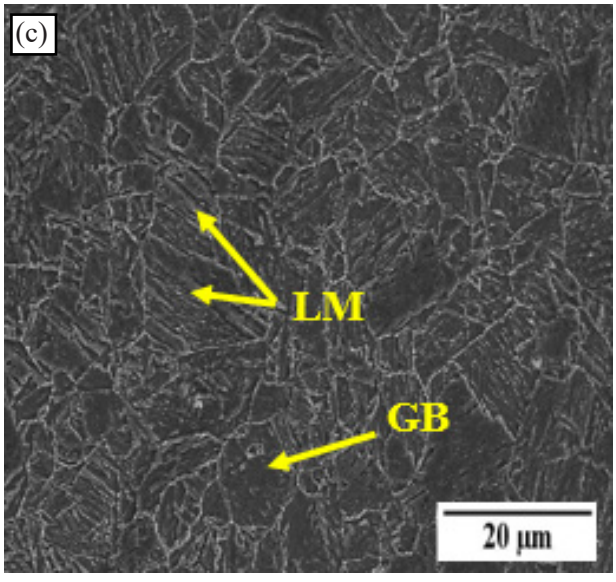

Fig. 2. HSLA-100 steel microstructure a) Optical microscope image (etched by 2% Nital solution) b) Optical microscope image (etched by Lepera solution) c) SEM image.

3.1.2. Weld metal microstructure

The microstructure of the weld metal obtained from ER120S-G filler metal has been depicted in different heat inputs in Fig. 3. The fig indicates that the weld metal microstructure in different heat inputs consists of acicular ferrite, polygonal ferrite, quasi-polygonal ferrite, and M/A constituent. The comparison of Figs. 3-a, 3-c, and 3-e shows that the weld metal microstructure is predominantly acicular ferrite in the entire heat inputs and that by increasing the heat input, its amount in the microstructure is decreased and the contribution of high-temperature ferrites such as polygonal (allotriomorphic) and quasi-polygonal ferrites is increased. Besides, it was observed that by increasing the heat input there occurs the coarsening of the phases and the existing compounds in the microstructure. In the low alloy steels, the austenite transformation into the ferritic microstructures with different morphologies begins when the temperature drops below the transformation temperature (Ar_3). At first, the polygonal ferrite starts to nucleate and grow on the austenite grain boundaries within the grains at high temperatures. As cooling continues to the lower temperatures, the polygonal ferrite grains commence to lose their regular shape, and the boundaries become jagged and uneven. This irregular shape is called quasi-polygonal or massive ferrite. By further cooling during solidification, the acicular ferrite nucleates and is formed on the inclusions in the austenite by a diffusional-shear mechanism [24-28].

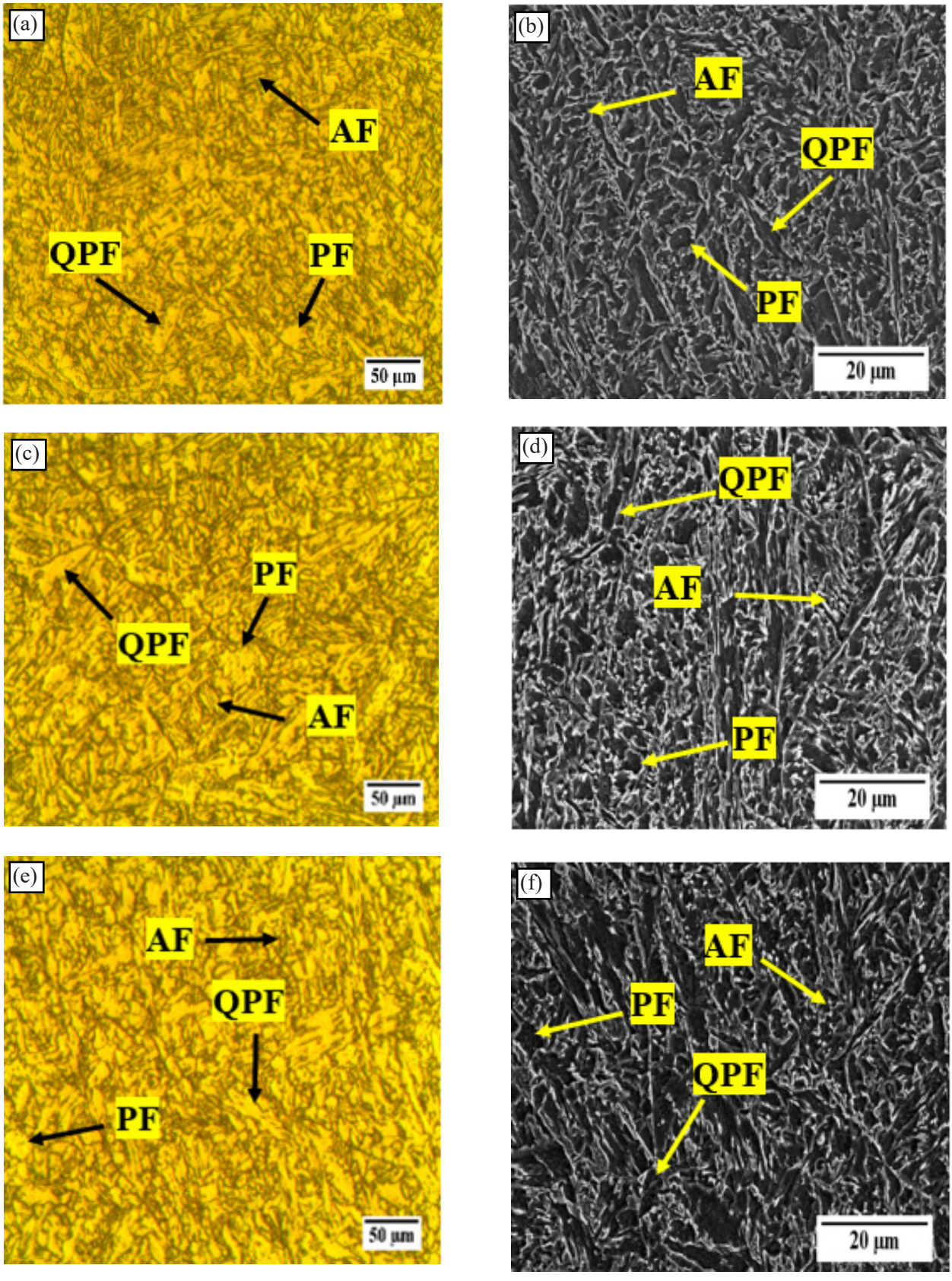

Fig. 3. Optical and SEM image of weld metal microstructure at the heat inputs of a&b) 0.78 kJ/mm c&d) 1.22 kJ/mm and e&f) 1.42 kJ/mm.

As it is known, the cooling rate is influenced by the heat input. Likewise, the cooling rate affects the type of microstructure of the weld metal and HAZ. In that is commonly used in the temperature range of 500-800 °C to show the cooling time. It can be calculated by the following empirical equation [19] :

$$\Delta t_{8/5}=5\eta.HI \qquad \text{Eq. (2)}$$

According to this equation, the cooling time depends on the heat input and arc efficiency, represented by H.I and η, respectively. It has been determined that by utilizing this equation, the cooling times of 2.34, 3.66, and 4.26 seconds are obtained for the heat inputs of 0.78 kJ/mm, 1.22 kJ/mm, and 1.42 kJ/mm, respectively. Therefore, based on these results, it is obvious that the cooling rate is raised by gaining the higher values of the heat input (the cooling time has become longer), and hence the ferritic microstructure size increases. Moreover, since the acicular ferrite is formed in a lower temperature range than the polygonal and quasi-polygonal ferrites, increasing the heat input followed by decreasing the cooling rate enhances the formation probability of higher temperature transformations products such as the polygonal ferrite; in contrast, the amount of acicular ferrite in the final microstructure is decreased.

The effect of the heat input on the morphology and distribution of the M/A constituent in the weld metals has been illustrated in Fig. 4. In the figure, the M/A constituent is observed with both the blocky and stringer morphologies at all heat inputs with a relatively uniform distribution. This indicates that the heat input variation has not affected the distribution and morphology of this secondary phase remarkably. Comparing the images showed that the blocky type M/A constituent content is increased relatively as higher heat inputs are applied. M/A constituents often are formed on the boundaries of acicular ferrite where the carbon-rich areas exist owing to the shear-diffusional mechanism of acicular ferrite formation. Hence, most of the formed M/A are distributed along the acicular ferrite boundaries with adjacent phases. Accordingly, due to more transformed acicular ferrites at lower heat inputs, the morphology of M/A in the matrix is mainly of stringer type. This can be considered as one reason for further blocky type M/A formation. Moreover, another reason for the M/A constituent morphology change from the stringer type to the blocky one at higher heat inputs can be attributed to an increase in the amount of polygonal and quasi-polygonal ferrites by increasing heat input. The formation of these two mentioned phases is associated with the carbon diffusion so that the blocky type M/A constituent may be formed within the grains and on the boundaries of polygonal and quasi-polygonal ferrites. The effect of various thermal cycles on the volume fraction of M/A constituent has been portrayed in Fig. 5. It has been depicted that the volume fraction of M/A constituent has been reduced in the microstructure at higher heat inputs. This can be attributed to the acicular ferrite coarsening by increasing the heat input. Thus, whereas the residual austenite is decreased by increasing the heat input, a lower amount of M/A constituent will be formed. Similar studies by other researchers [29] have shown that the smaller the size of the acicular ferrite is, the greater the amount of surrounding residual austenite exists. Since the heat input is increased, the amount of residual austenite decreases, and the formation of a smaller volume fraction of M/A constituent is expected.

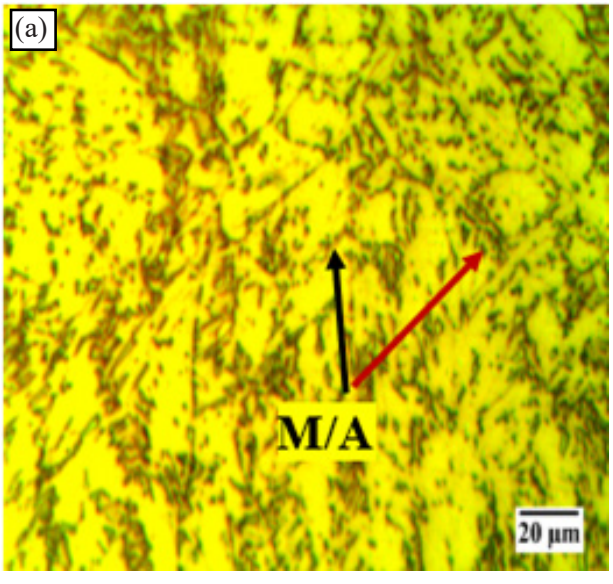

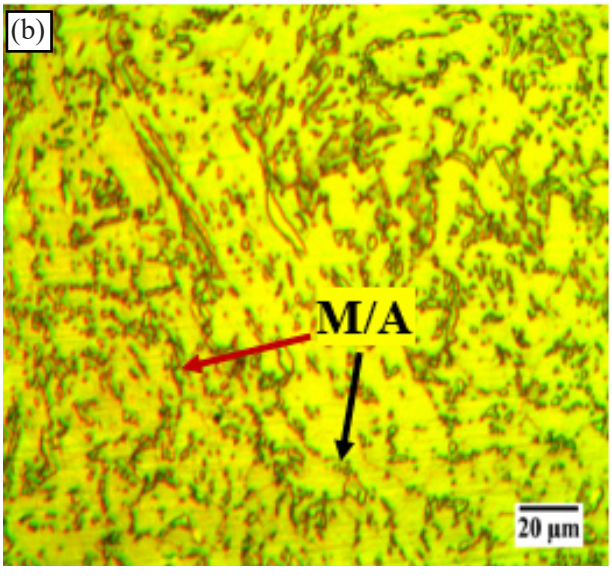

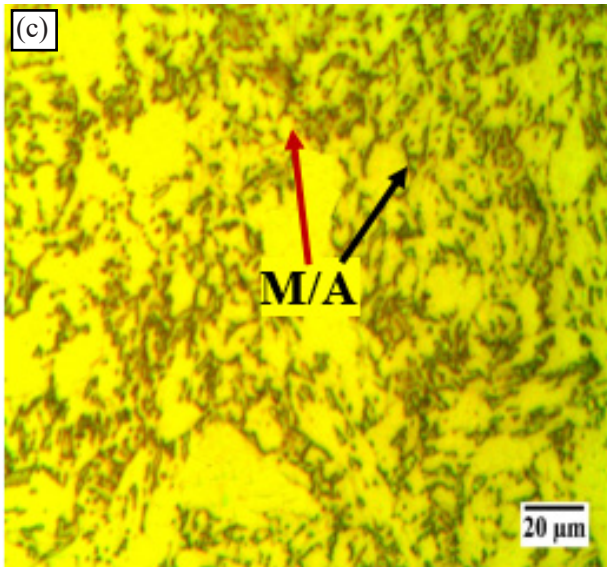

Fig. 4. M/A secondary phase distribution in the weld metal microstructure at various heat inputs of a) 0.78 kJ/mm b) 1.22 kJ/mm C) 1.42 kJ/mm. Blocky and stringer M/A constituents were indicated by red and black arrows, respectively.

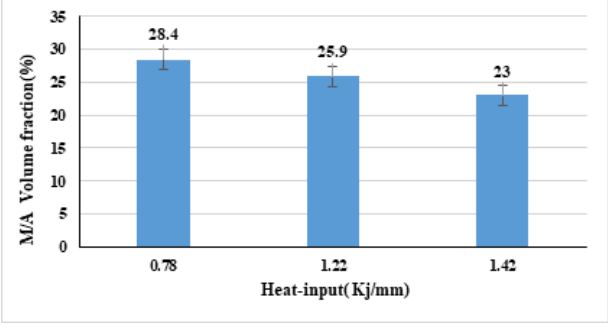

Fig. 5. The effect of heat input on M/A constituent volume fraction in weld metals.

3.2. Heat-affected zone microstructure

The microstructure of various joint zones (weld metal, interface and, HAZ) has been represented in Fig. 6 in different thermal cycles. It has been observed that the interface is fully continuous between the base metal and the weld zone without any cracks and discontinuities for all heat inputs. Besides, in all specimens an epitaxial growth from semi-melted grains in the fusion line is clearly observed. The epitaxial growth occurs when the base and filler metal have a close chemical composition, a similar crystal lattice, and a slight difference at the melting point [30]. Hence, based on the similarity of the chemical composition of base metal and welding consumable (Table.1), an epitaxial growth mechanism seems reasonable.

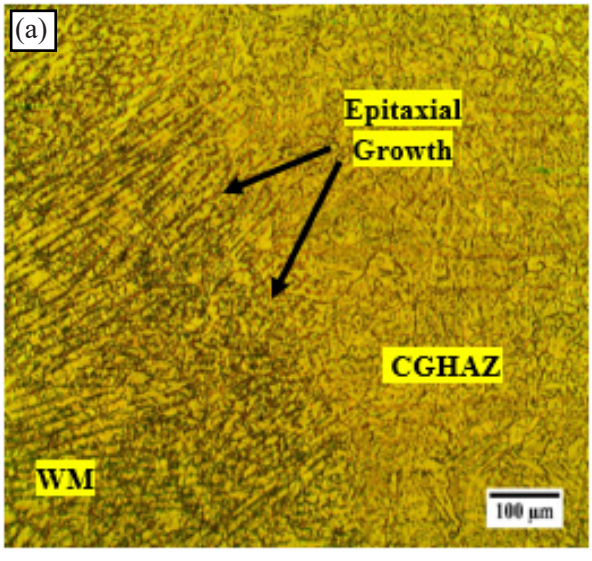

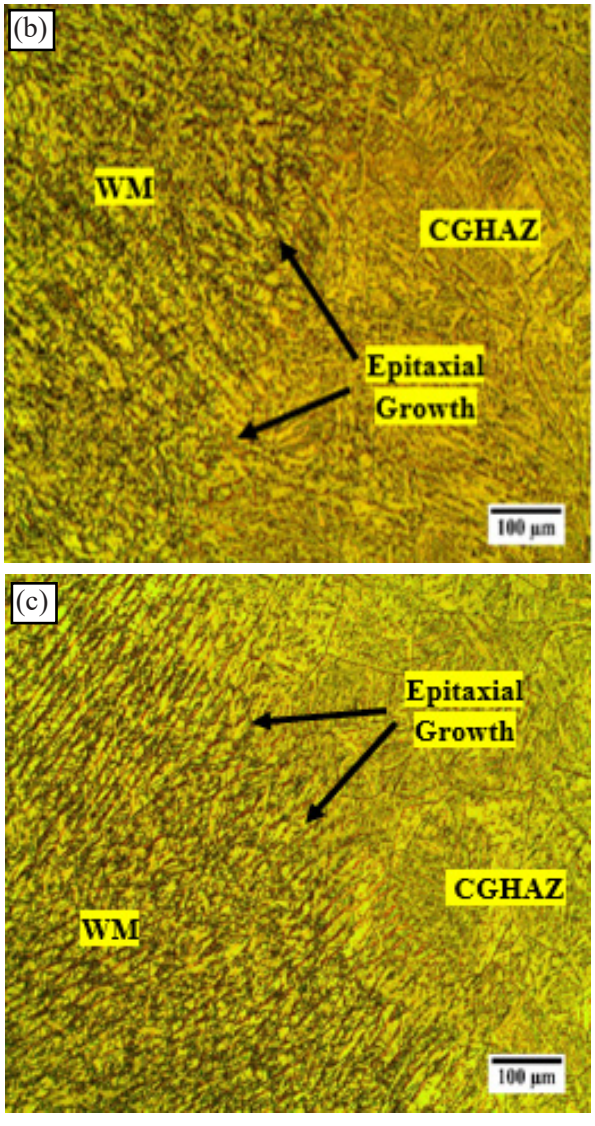

Fig. 6. Interface between weld metal and HSLA-100 base metal at heat inputs of a) 0.78 kJ/mm b) 1.22 kJ/mm c) 1.42 kJ/mm.

The grain size change is clearly observed in the HAZ at all heat inputs. Based on the grain size and the microscopic observations, two different regions were distinguished in the heat-affected zone, namely coarse-grained and fine-grained zones. The coarse-grained zone is formed exactly next to the fusion line. This zone can be seen in Fig. 6 a-c. In terms of nomenclatures, the coarse-grained and fine-grained areas in the heat-affected zone have been represented as CGHAZ and FGHAZ, respectively. It is also observed that CGHAZ has been extended further by an increase in the heat input. The microstructural images of CGHAZ and FGHAZ have been exhibited at higher magnification in Figs. 7 and 10, respectively. Fig. 7 demonstrates that the CGHAZ microstructure comprises granular and lath Bainites (LB) with the M/A secondary phase. The granular bainite has a ferritic matrix (bianitic ferrite) during whose formation the M/A secondary phase is distributed within the ferrite grains [31]. The lath Bainite also has coextensive ferrite sheaves, between which the M/A constituent is formed. In this type of bainite, the ferrite sheaves have the same direction starting to grow anisotropically from the prior austenite grain boundaries (PAGB) and continuing their growth within the grains [32,33].in contrast, The granular bainite microstructure is formed within austenite grains by the edge growth mechanism [34]. This factor, which provides appropriate conditions for the observing of the primary austenite grain boundaries, has been distinguished conspicuously in Fig.7. The lath bainite is formed in the lower temperature range than the granular Bainite [34]. According to Fig. 7-a, the dominant microstructure of CGHAZ in the heat input of 0.78 kJ/mm contains the granular bainite with a small amount of lath Bainite. As the heat input (Fig. 7-b and c) is increased and followed by a slower cooling rate, the lath bainite amount is augmented significantly. Increasing the amount of lath bainite in the microstructure is due to the further dissolution of impurities, copper precipitates, and niobium carbonitrides because of the heat input enhancement, which results in acquiring more homogeneous austenite with further hardenability. Because of achieving more hardenability, the amount of lower temperature transformed phase (lath Bainite) is increased. The comparison of the microstructures in Fig.7 shows that an increase in the heat input is accompanied by the austenite grain size propagation in CGHAZ. The consequence of the austenite grain size measurement shown in Fig. 8 shows that the austenite grain size is elevated from 29.2 µm to 76.5 µm by augmenting the heat input from 0.78 kJ/mm to 1.42 kJ/mm. This can be attributed to the Niobium carbonitrides dissolution. These precipitates prevent the growth of the prior austenite grains due to the grain boundary pinning effect [35]. Therefore, the incremental trend of the prior austenite grains size is carried on by the dissolution of carbonitride precipitates, resulting in high heat inputs. As the heat input ascends, the temperature near the fusion line is raised, and more time is provided for the carbon diffusion from the degenerated ferrite into the austenitic matrix. This factor has contributed to further austenite stability and increased the M/A constituent volume fraction from 9.2 to 19.6 percent at the heat inputs of 0.78 kJ/mm and 1.42 kJ/mm, respectively (Fig. 9). This increase in the volume fraction of the M/A constituent with the heat input increment has also been reported in the studies carried out by other researchers [36, 37]. Fig. 10 shows the microstructure of FGHAZ at different heat inputs. It has been demonstrated that this zone microstructure is mainly made up of the granular bainite, which possesses the M/A constituent and whose size has grown by the heat input increment. Besides, some lath bainite has been formed in the maximum heat input (1.42 kJ/mm),

whose formation is due to the additional dissolution of the carbonitride precipitations in austenite. Furthermore, the results of austenite grains measurement presented in Fig. 8 determines that the austenite grains size in the FGHAZ has increased from 15.7 µm at the heat input of 0.78 kJ/mm to 32.2 µm at the heat input of 1.42 kJ/mm.

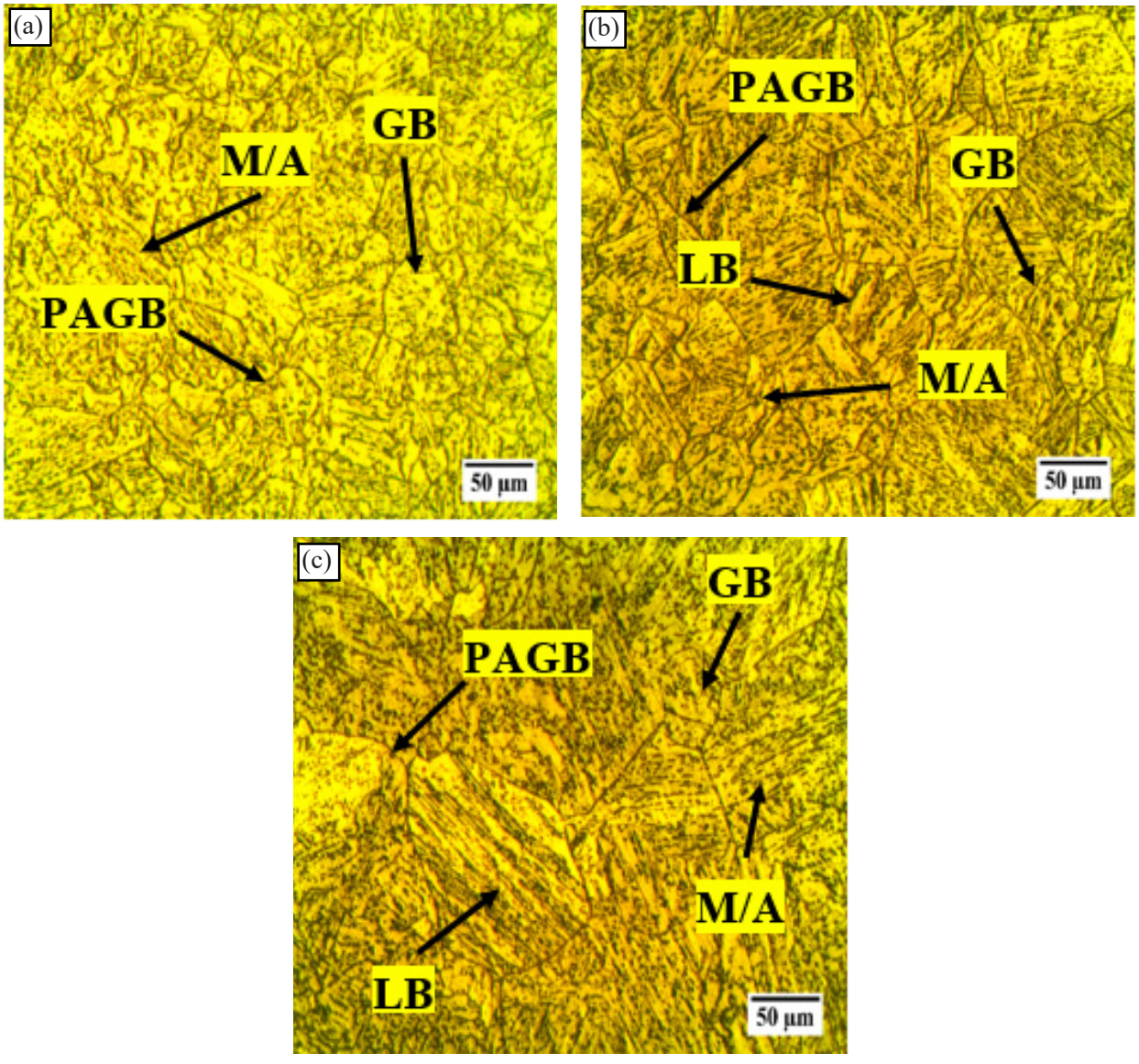

Fig. 7. CGHAZ microstructure at different heat inputs of a) 0.78 kJ/mm b) 1.22 kJ/mm c) 1.42 kJ/mm.

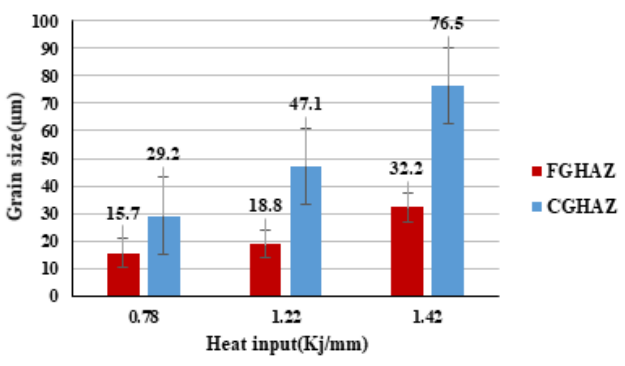

Fig. 8. Prior Austenite grain size in CGHAZ and FGHAZ at different heat inputs.

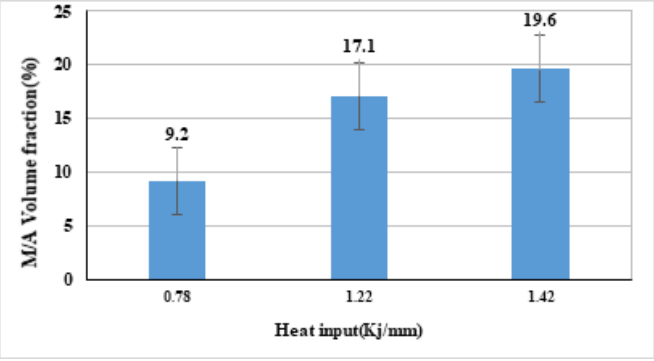

Fig. 9. M/A constituent volume fraction in the CGHAZ at various heat inputs.

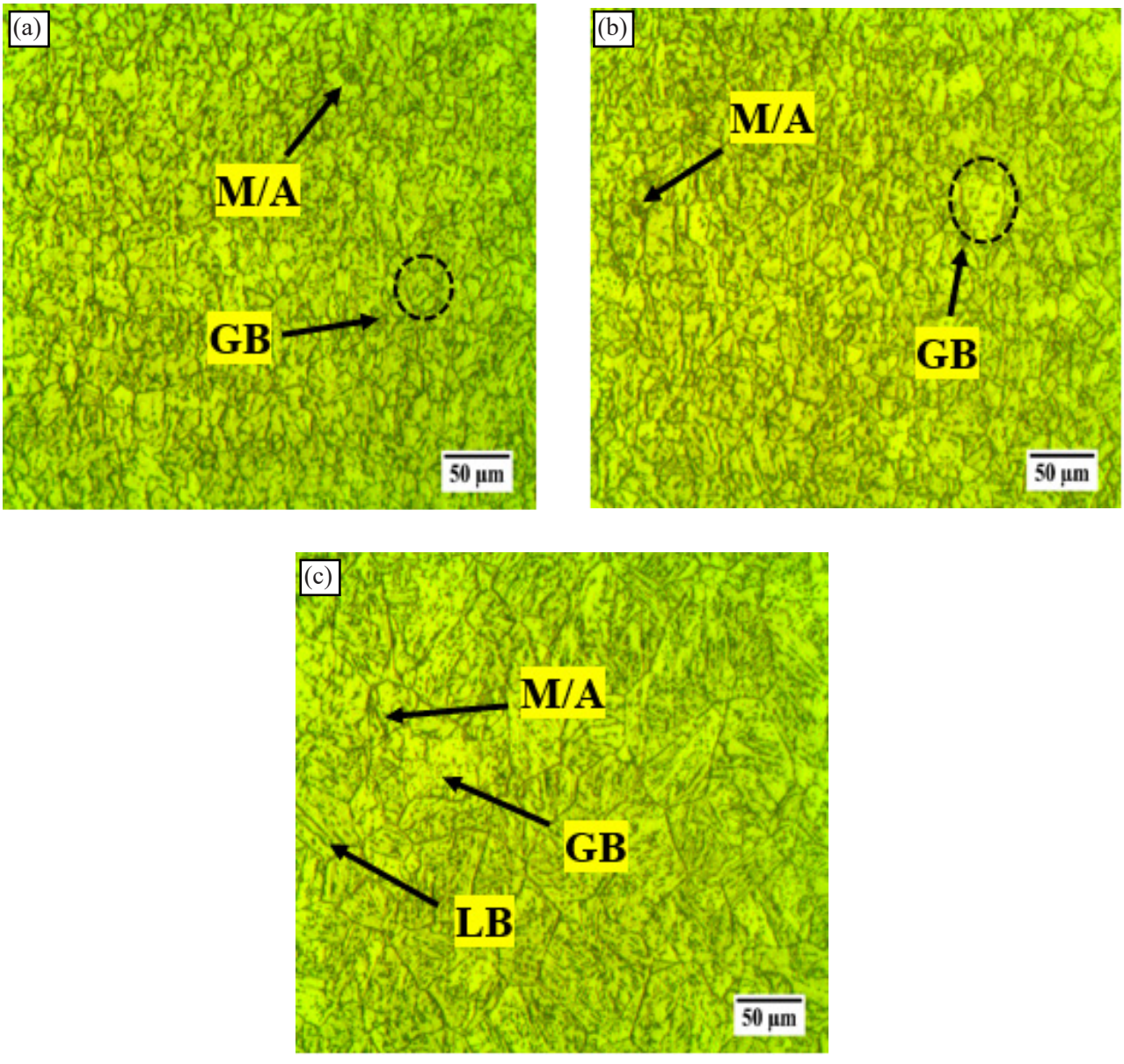

Fig. 10. FGHAZ microstructure at different heat inputs of a) 0.78 kJ/mm b) 1.22 kJ/mm c) 1.42 kJ/mm.

In the FGHAZ, the temperature rises to the single-phase austenite region, and the austenitization process occurs completely. Due to the lower maximum temperature in FGHAZ than in CGHAZ, the dissolution of carbonitride precipitates does not take place entirely. The incomplete dissolution of precipitates can be considered as a factor against the grain growth in FGHAZ, and finer grains can be formed in this zone compared to CGHAZ. Due to the lower temperature of FGHAZ than CGHAZ, the austenite homogeneity and consequently its hardenability is reduced so that this factor can overcome the higher cooling rate of FGHAZ, thereby creating phases such as granular bainite with lower hardness compared to CGHAZ with the lath bainite predominant microstructure. The effect of soft phases in the FGHAZ hardness in the microhardness profile diagram has been revealed in Fig. 11. Based on this diagram, it can be clearly seen that the lowest hardness is achieved in the FGHAZ.

To measure the temperature changes in the HAZ, Fig. 12 indicates the recorded thermal cycles obtained from thermocouples implantation at different distances from the fusion line. Due to the temperature range of the CGHAZ and FGHAZ mentioned in the literature [38,39], it is expected that austenitization occurs thoroughly in both regions. The empirical equations (3) and (4) are used to calculate the AC_1 and AC_3 temperatures of HSLA-100 steel. Based on these equations and the HSLA-100 steel chemical composition used in this research, the values of AC1 and AC3 are obtained as 719.6°C and 837.7°C, respectively.

$$Ac_1(^{\circ}C) = 723 - 10.7Mn - 3.9Ni + 29Si + 16.7Cr + 290As + 6.38W \quad \text{Eq.(3}$$

$$Ac_3(^{\circ}C) = 910 - 230C^{0.5} - 15.2Ni + 44.7Si + 104V + 31.5Mo + 13.1W \quad \text{Eq.(4)}$$

It can be seen in Fig. 12 that the maximum temperature for each thermocouple rises by raising the heat input so that the first thermocouple maximum temperature reaches 898.2 °C, 1021.4°C, and 1194.6 °C for the heat inputs of 0.78 kJ/mm, 1.22 kJ/mm, and 1.42 kJ/mm, respectively(fig. 13). In addition, it was found that by increasing the heat input, the exposure time of each thermocouple at high temperature rises. Subjection to high temperatures above AC_3 in FGHAZ and CGHAZ, along with complete austenitization, leads to the precipitates dissolution and more grain growth (as illustrated in Fig. 7 and Fig. 10). Another effect of experiencing high temperature besides the grain growth and peak temperature increase for each thermocouple at farther distances from the fusion line by increasing the heat input depicted in Fig.13 is the extension of the HAZ width. It was ascertained that the width of the heat-affected zone had been increased from 3.6 mm to 4.5 mm for the heat input increase from 0.78 Kj/mm to 1.42 Kj/mm.

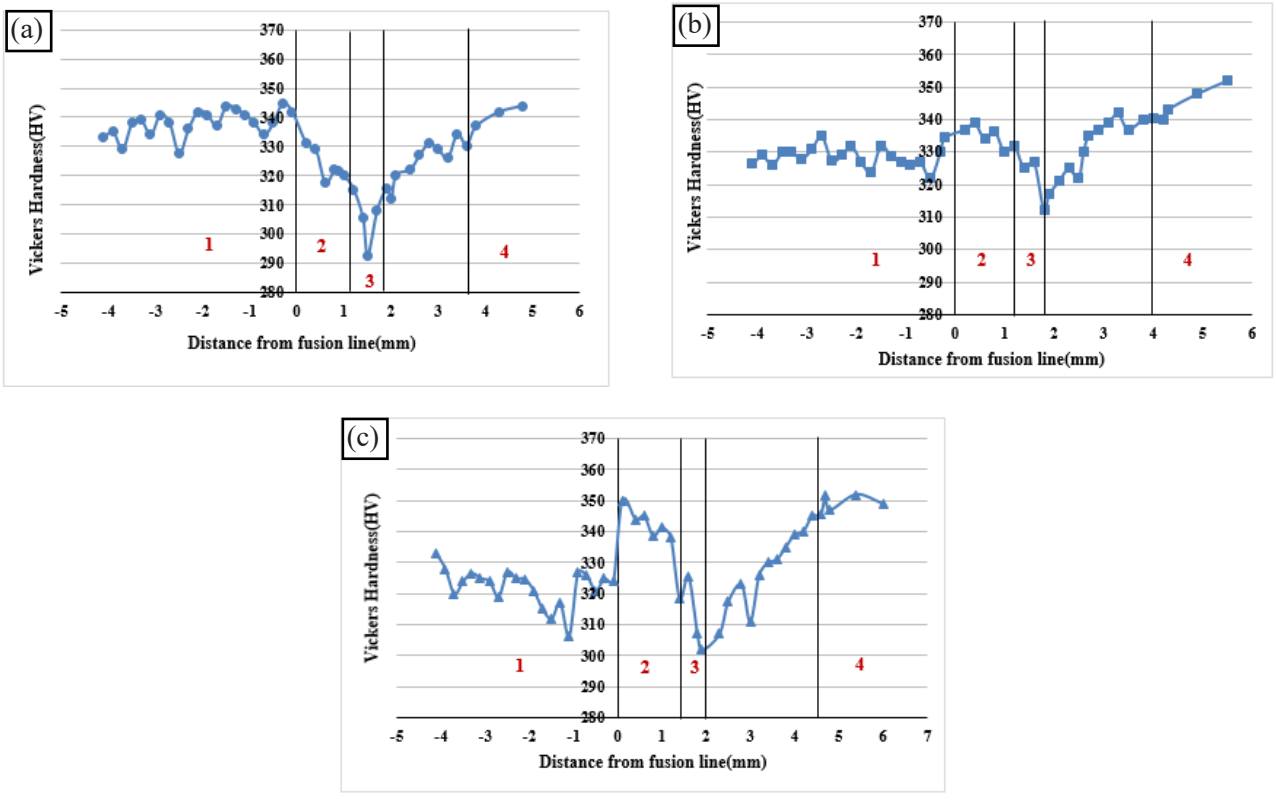

Fig. 11. Hardness distribution in different joint areas at various heat inputs of a) 0.78 kJ/mm b) 1.22 kJ/mm c) 1.42 kJ/mm 1: Weld metal, 2: Coarse-grained zone, 3: Fine-grained zone, 4: Base metal..

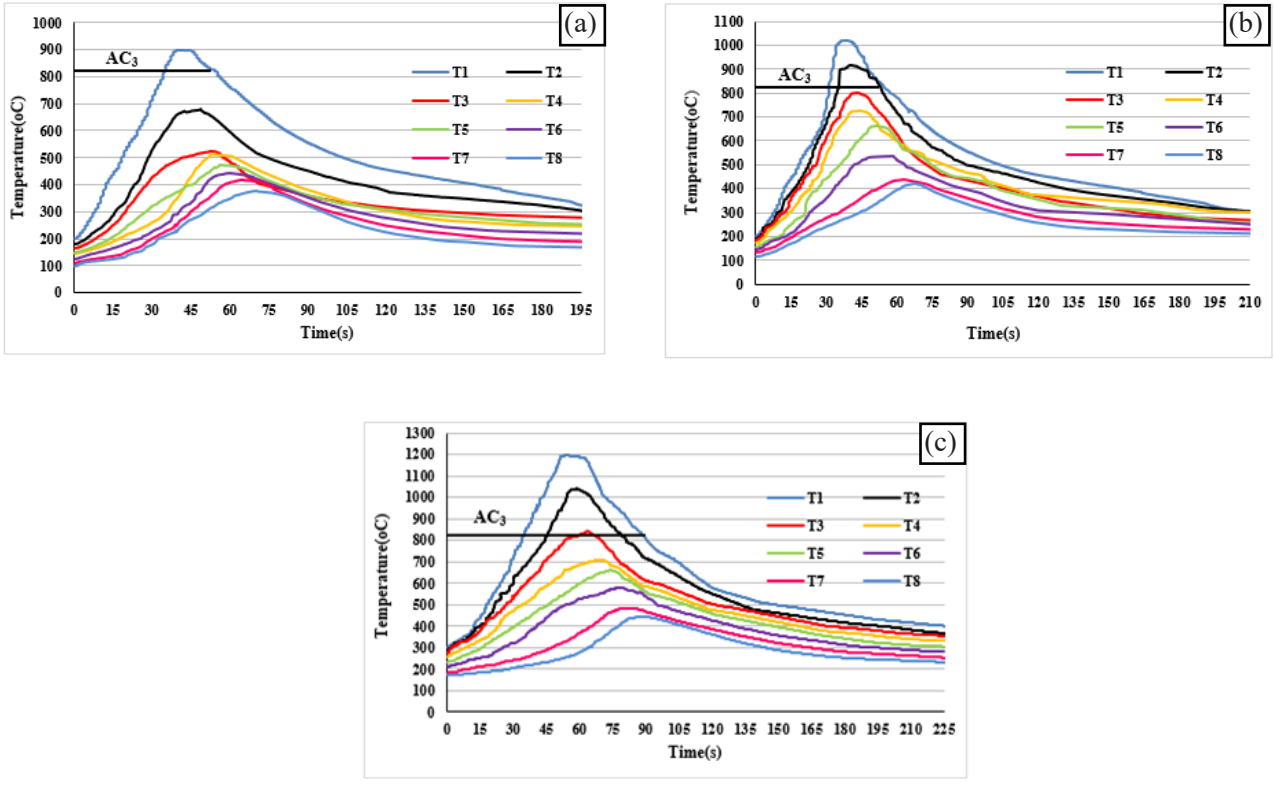

Fig. 12. Welding thermal cycles at different heat inputs of a) 0.78 kJ/mm b) 1.22 kJ/mm c) 1.42 kJ/mm.

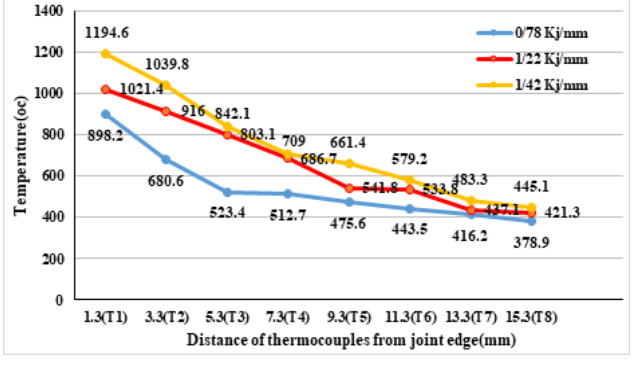

Fig. 13. Maximum temperature changes at different distances from the fusion line at various heat inputs.

4. Conclusion

- It was found that the HSLA-100 steel base metal microstructure consists of the granular bainite, lath martensite, and M/A constituent. In contrast, the ER120S-G weld metal microstructure is composed of acicular, polygonal, and quasi-polygonal ferrites with M/A constituents.
- The interfaces between the base and weld metal were fully continuous at all heat inputs, and no cracks and discontinuities were observed. an epitaxial growth occurred at various heat inputs at the interface between the base metal and the weld metal.
- The heat-affected zone was divided into two parts of CGHAZ with the granular bainite, and lath bainite microstructure, and FGHAZ with the granular bainite predominant microstructure. Besides, the formation of M/A constituent was observed in both FGHAZ and CGHAZ.
- By increasing the heat input, the acicular ferrite amount in the weld metal microstructure was decreased, and the contribution of polygonal and

quasi-polygonal ferrites was increased. It was found that the M/A constituent volume fraction in the weld metal declines by increasing the heat input. In contrast, the blocky type of M/A constituent amount increases slightly in comparison with the stringer one.

- Increasing the heat input from 0.78 Kj/mm to 1.42 kJ/mm caused an increase in the prior austenite grain size from 29.2 μm to 76.5 μm in CGHAZ and from 15.7 μm to 32.5 μm in FGHAZ.
- Using the temperature-time thermal cycles, it was specified that the heat-affected zone width is expanded from 3.6 mm to 4.5 mm as the heat input rises from 0.78 kJ/mm to 1.42 kJ/mm.

References

[1] B. K. Show, R. Veerababu, R. Baramuralikrishnan, G. Malakondaiah: Mater. Sci. Eng. A., 527(2010), 1595.

[2] Y. Liu, L. Shi, C. Liu, L. Yu, Z. Yan, H. Li: Mater. Sci. Eng. A., 675(2016), 371.

[3] S. Vervynckt, K. Verbeken, B. Lopez, J.J. Jonas: Int. Mater. Rev., 57(2012), 187.

[4] S. K. Dhua, D. Mukerjee, D. S. Sarma: Metall. Mater. Trans. A., 34(2003), 2493.

[5] S. K. Dhua, D. Mukerjee, D. S. Sarma: Metall. Mater. Trans. A., 32(2001), 2259.

[6] S. Das, A. Ghosh, S. Chatterjee, P. R. Rao: Scand. J. Metall., 31(2002), 272.

[7] M. Mujahid, A. K. Lis, C. I. Garcia, A. J. Deardo: J. Mater. Eng. Perform, 7(1998), 247.

[8] E. J. Czyryca, M. G. Vassilsros: Ship. Mater. Eng. Depart. Res. Develop. Rep., 1993.

[9] G. Thewlis: Mater. Sci. Technol, 20(2004), 143.

[10] S. Kou: Welding metallurgy, John Wiley and Sons, New Jersey, (2003), 145.

[11] S. S. Babu: Curr Opin Solid State Mater Sci, 8(2004), 267.

[12] X. J. Di, X. An, F. J. Cheng, D. P. Wang, X. J. Gou, Z. K. Xue: Sci. Technol. Weld. Join, 21(2016), 366.

[13] Y. Li, T. N. Baker: Mater. Sci. Technol., 26(2010), 1029.

[14] G. Spanos, D. W. Moon, R.W. Fonda, E. S. K. Menon, A. G. Fox: Metall Mater Trans A, 32(2001), 3043.

[15] K. Prasad, D. Dwivedi: Int. J. Adv. Manuf. Technol., 36(2008), 475.

[16] B. Beidokhti. A.H. Koukabi, A. Dolati: Mater Charact, 60(2009), 225.

[17] M. Shome: Mater. Sci. Eng. A., Vol (2007), 454.

[18] M. Shome, O. N. Mohanty: Metall Mater Trans A, 37(2006), 2159.

[19] H. Dong, X. Hao, D. Deng: Metallogr. Microstruct. Anal., 3(2014), 138.

[20] ASME Sec IX, American Society of mechanical engineers: Qualification Standard for Welding and Brazing Procedure, Article II, Welding Procedure Qualification, 2015.

[21] E. Girault, P. Jacques, Ph. Harlet, K. Mols, J.Van Humbeeck, E. Aernoudt, F. Delannay: Mater Charact, 40(1998), 111.

[22] ASTM E112, American Society for Testing and Materials: Standard test method for determining average grain size, 2004.

[23] S. S. Ghasemi banadkouki, D. P. Dunne: ISIJ Int., 46(2006), 759.

[24] O. Grong, D. K. Matlock: Int. Met. Rev., 31(1986), 27.

[25] Z. Zhang, R.A. Farrar: Mater. Sci. Technol., 12(1996), 237.

[26] J. M. Dowling, J. M. Corbett, H .W. Kerr: Metall. Mater. Trans. A., 17(1986), 1611.

[27] S. Panwar, D. B. Goel, O.P. Pandey, K. Satya Prasad: Bull. Mater. Sci., 29 (2006), 281.

[28] L. Lan, C, Qiu, D. Zhao, X. Gao, L. Du: J. Mat. Sci., 47(2012), 4732.

[29] I. A. Yakubtsov, J. D. Boyd: Mater. Sci. Technol., 17(2001), 296.

[30] H. Inoue, T. Koseki, S. Okita, M. Fuji: Weld. Int., 12(1998), 195.

[31] H.J. Jun, J.S. Kang, D.H. Seo, K.B. Kang, C. G. Park: Mater. Sci. Eng. A., 422(2006), 157.

[32] X. Li, C. Shang, X. Ma, B. Gault, S.V. Subramanian, J. Sun, R.D.K. Misra: Scr. Mater., 139(2017), 67.

[33] S. Moeinifar, A. H. Kokabi, H. R. Madaah Hosseini: Mater. Des., 31(2010), 2948.

[34] C. Sun, S. Yang, G. Liu: Acta Metall. Sin(Engl. Lett.), 27(2014), 426.

[35] S. D. Bhole, A. G. Fox: Can. Metall. Q., 35(1996), 151.

[36] A. Lambert-perlade, A.F. Gorgoues, J. Besson, T. Sturel, A. Pineau: Metall. Mater. Trans. A., 35(2004), 1039.

[37] S. Moeinifar, A. H. Kokabi, H .R. Maadaah Hosseini: J Mater Process Technol, 211(2011), 368.

[38] S. Moeinifar, A. H. Kokabi, H. R. Madaah Hosseini: Mat. Des., 31(2010), 2948.

[39] K. W. Andrews: ISIJ Int., 203(1965), 721.